

# PERFORMANCE ANALYSIS OF MODIFIED TERRAIN PROPAGATION MODELS AGAINST THEIR REFERENCE MODELS IN TERMS OF SPEED AND ACCURACY

A. S. Owadally and S. R. Saunders

University of Surrey, UK.

## 1 INTRODUCTION

Wave propagation modelling is a key component in the design of cellular mobile communications networks. Two of the critical parameters in a propagation tool are its computational speed and accuracy. Ideally, the radio-planning engineer seeks for an appropriate combination of both parameters. However, very often, a compromise has to be made between these two aspects, which is often guided by the specific system needs and the link margin available.

In order to address these needs, this paper investigates two models that are modifications of some existing models to improve their speed-vs-accuracy performance. As reference terrain propagation models, the narrow angle parabolic equation (NAPE) (1) and the slope-UTD model (STD-UTD) (2) are used. In principle a full-wave model is more accurate than a canonical model since the terrain profile is better taken into account. However by the same token, a canonical model is faster.

In the next section of this paper, we will describe the modified models, namely the NAPE-FS (free-space) and the Selected Edges UTD (SE-UTD) model. An evaluation of their performance against their reference models will be carried out by comparing predictions with measurements for profiles from a terrain database in Aalborg, Denmark (3). Conclusions drawn from the set of results will then be outlined.

## 2 MODIFIED MODELS

**NAPE-FS.** The NAPE-FS model is essentially the NAPE model (using an absorbing layer at the upper boundary), but fed with different input data. The NAPE-FS represents an attempt to speed up the NAPE by focusing on segments of terrain, which are more significant in terms of diffraction effects. These significant regions represent an approximation to the full terrain profile and free-space propagation is assumed in between.

The minimum Fresnel propagation region (MFPR) is used as a gauge to decide whether an edge is treated as a significant obstruction or not. As defined by Hristov (4), the MFPR is equivalent to 0.6 of the first Fresnel zone. The total path loss between the transmitter (Tx) and the receiver (Rx) will be quite similar to an unobstructed case if there are no edges in MFPR. Therefore, the idea is to check whether each edge

occurs inside or outside the MFPR. The edge selection in the NAPE-FS model is described below:

A. The terrain profile between a Tx and a Rx can be approximated to a series of knife edges, assuming that the variation in the terrain is on a scale smaller than the wavelength of interest. As a first step, we will identify a number of significant (or main) edges given by, *num\_sig\_edges (nse)*. These will be selected from the terrain profile between the Tx and the Rx. The main edges are deemed to be significant in terms of their diffractive effects and will be selected based on Vogler's  $\beta$  parameter (5). A description of this selection will be given in the next sub-section.

B. The main edges will be considered as "virtual" transmitters and receivers. The MFPR is drawn across each pair of main edges and where relevant, between the "real" transmitter/receiver and a main edge. We then assess whether each terrain edge in between a pair of main edges, occurs within the MFPR. If an edge lies within the MFPR, this edge is assumed to have a significant contribution to the net path loss. As a result, this edge is considered to be part of a significant region. On the other hand, if an edge lies outside the MFPR, its diffractive effect is deemed to be minimal and it is excluded from the significant regions

In the NAPE-FS model, the NAPE model is run over the significant regions. Clusters of edges that are excluded from the significant regions, are approximated to free-space (FS) regions

The propagation through free-space (FS) is achieved by a heuristic implementation of the Fresnel-Huygens' principle. As shown in Fig 1, we will consider the field at the FD grid points along the start vertical of the FS zone as cylindrical sources. The aim is to find the contribution of each of the above cylindrical sources at each of the FD grid points along the end vertical of the FS zone. Hence the field at the topmost grid point, X, along the end vertical, is given by the summation of the contribution of the sources,  $E_1^s, \dots, E_4^s$  at that point X.

$$E_4^c = \left[ (E_1^s \cdot \phi(\rho_{14})) + (E_2^s \cdot \phi(\rho_{24})) + (E_3^s \cdot \phi(\rho_{34})) + (E_4^s \cdot \phi(\rho_{44})) \right] \cdot 4\pi \quad [1]$$

where  $\phi(\rho) = (j/4)H_0^{(1)}(k_\rho \rho)$ , which is a solution to a wave equation with a cylindrical source,  $\rho$  is the radial distance from the source to the measuring point and  $H_0^{(1)}(\ )$  is the Hankel function of the first kind and zeroth order

A formulation along the lines of [1] is used to calculate the field at other grid points along the end vertical of the FS zone. This process is repeated across each FS zone occurring within the profile. Hence, the inclusion

of the FS zone brings about a saving in computational time, albeit at the expense of prediction accuracy since the effects of some obstacles are ignored.

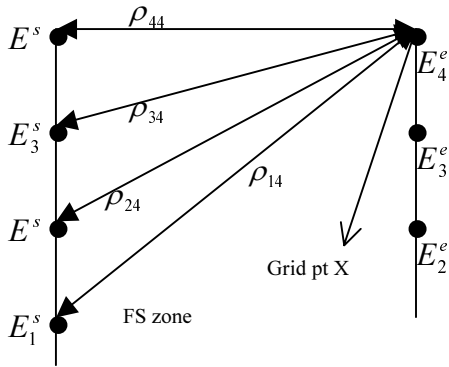


Fig 1. Schematic showing grid pts at the start and end verticals of the FS zone

**SE-UTD.** The only difference between the SE-UTD and STD-UTD models lies in the input data selection. The edge selection in the SE-UTD model is expected to take into account a more global shape of the terrain profile, in addition to its local variation, whilst only the latter is considered in the STD-UTD case. As a result, it is hoped that the above difference in edge selection between the two models will translate into a more accurate prediction being made by the SE-UTD model. A detailed description of the steps in the edge selection approach within the SE-UTD model is given below:

I: A number of significant (or main) edges given by,  $nse$ , is identified from the set of knife-edges that represents the whole terrain. The total number of edges is reduced to  $nse$ , in the following way: The  $\beta$  parameter of each edge in the profile is evaluated based on the relative heights and distances of that edge with its adjacent edges. The edge with the most negative  $\Re[\beta]$ , say edge B, is deemed to have the least contribution to the diffraction loss (5). Hence this edge is not of interest and should be ignored. The  $\beta$  parameter is then recalculated for the edges adjacent to B, say edges A and C, assuming B is absent. The newly calculated  $\beta$  parameter for edges A and C is compared with those of the remaining edges in the profile. The same elimination process as above is repeated until the total number of edges is given by  $nse$ .

II: Ellipsoids representing the MFPR are drawn across pairs of main edges and the Tx and Rx. We then determine which edges in the terrain profile are within the MFPR. As before, the edges within the MFPR are deemed to be significant in terms of diffraction loss.

III: Usually the number of edges within the MFPR is quite high. They are narrowed down to a number given by  $final\_num\_sig\_edges$  ( $fnse$ ), by determining the most significant edges based on Vogler's  $\beta$  parameter. It should be noted that the edge selection in the STD-UTD model consists of stage I only. In the STD-UTD model,  $nse$  has an upper limit of 8, and if the change in diffraction loss due to  $i+1$  edges is greater than 0.1 dB relative to that for  $i$  edges, then the number of optimum

edges is chosen to be  $i+1$ . From the description of stage I, it is clearly seen that an edge is assessed based on its diffractive effects with respect to its immediate adjacent edges. Hence in some ways it can be said that the edge selection in the STD-UTD model is more focused on the local diffractive effects of an edge. By including stage II in the edge selection process of the SE-UTD model, the method attempts to take into account the diffractive effect of an edge with respect to an adjacent pair of main edges that may not be situated locally to the edge in question. It is thus expected that a more global perspective will be taken whilst carrying out edge selection.

### 3 RESULTS

The reference and modified models were run on the profiles of (3) at the frequency of 970 MHz. The chosen profiles are such that all the reception points in a profile can be assumed to lie in a 2D plane resulting in a point-to-multipoint collinear scenario. The accuracy of the models will be assessed based on (i) the root mean square of the error,  $E_{rms}$ ; where the error is defined as the difference between the measurements and the predictions. (ii) the mean of the Total Hit Rate (6),  $THR_m$ , which is the average of the non-100% values of the THR. A comparison of the performance of the modified models against their reference models will be shown for two profiles in the Aalborg database; Handsund and Mjels.

**Handsund profile: NAPE-based results.** The NAPE has been run for a range of values of upper boundary height,  $height\_dom$ , and the optimum value in terms of computational speed and accuracy was found to be 120m. This has then been used in the NAPE-FS model that was run for a range of  $nse$  from 1 to 5 (see Table 1)

$nse$	Time	NAPE-FS		Selected NAPE	
		$E_{rms}$	$THR_m$	$E_{rms}$	$THR_m$
	[min]	[dB]	[%]	[dB]	[%]
1	1.270	8.625	87.567	10.275	84.036
2	1.278	8.625	87.567	10.275	84.036
3	1.272	8.625	87.567	10.275	84.036
4	1.276	8.765	87.255	10.203	84.189
5	1.273	8.765	87.355	10.203	84.189

Table 1: Speed and accuracy of the NAPE-FS and NAPE predictions selected at significant regions, in the Handsund profile.

The NAPE-FS ( $nse = 3$ ) brings a gain in runtime of 65% compared to the NAPE (with  $height\_dom = 120m$ ). This gain in time may be quite useful to the radio-planning engineer when running simulations for a point to multipoint non-collinear scenario.

To gauge the accuracy of the NAPE-FS model, we have compared the former to NAPE predictions (with  $height\_dom = 120m$ ) selected only within the significant regions corresponding to each value of  $nse$ . The first order statistics and hit rate metrics for these selected predictions are referred to as the *selected NAPE* results and are shown in Table 1. The NAPE (with  $height\_dom = 120m$ ) prediction is chosen as a

comparator because it has the same value of  $height\_dom$  as the one used in the NAPE-FS simulations. Hence in principle, any difference in results from the two models will be inherent to the NAPE-FS concept. It can be seen that the NAPE-FS performs better than the NAPE in terms of accuracy: the  $E_{rms}$  of the NAPE-FS predictions is less than those of the selected NAPE predictions by a couple of dB. Also the  $THR_m$  for the NAPE-FS predictions is about a couple of percent better than the corresponding one for the selected NAPE prediction. These observations suggest that the NAPE-FS model is better than the NAPE model. In fact, the opposite was expected. This is because the NAPE takes into account the diffraction effects of the whole profile whilst the NAPE-FS model ignores certain segments of the profile. Fig 2 allows us to understand that the above observations stem from the following aspects: (i) The NAPE predictions within the significant regions, generally underestimate the path loss with respect to the measurements. (ii) The NAPE-FS predictions underestimate the path loss to a lesser extent than the NAPE predictions.

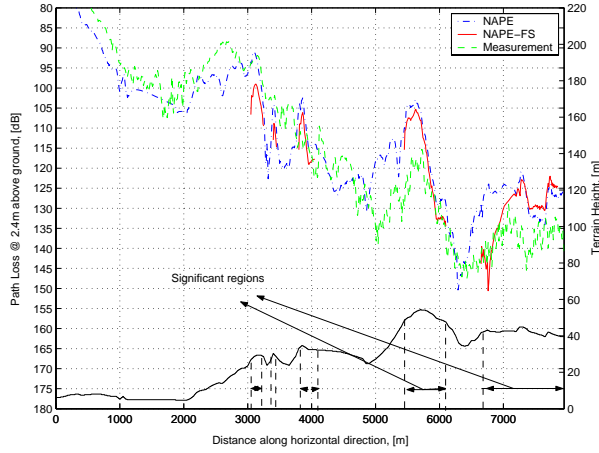


Fig 2. Measurement and predictions from the NAPE and NAPE-FS models for the Handsund profile.

Hence the NAPE-FS predictions are “closer” to the measurements. Item (ii) can be explained as follows: The free-space (FS) zones occur over segments of the profile where the diffraction losses are negligible. Hence the difference between the NAPE and the NAPE-FS predictions does not originate mainly from diffractive effects. In the NAPE-FS model, there is no reflection off the ground in the FS zones since we assume free-space. Hence the field strength as predicted by the NAPE-FS model may be weaker than the NAPE model, thereby resulting in item (ii).

**Handsund profile: UTD-based results.** The SE-UTD model with a value of  $nse = 3$ , has been run over the following segment of the Handsund profile: from 4.0km to 7.95km for a range values of  $fnse$  from 5 to 10 and the results are shown in Table 2. The SE-UTD is compared to the STD-UTD when the same  $fnse$  is used. STD-UTD predictions for the same values of  $fnse$  as used in the SE-UTD, will be referred to as *extended STD-UTD* predictions. If the same number of edges is being used in each model, then any gain in accuracy

will be due to the edge selection process and not the number of edges used.

$fnse$	SE-UTD			Extended STD-UTD		
	Time [min]	$E_{rms}$ [dB]	$THR_m$ [%]	Time [min]	$E_{rms}$ [dB]	$THR_m$ [%]
5	0.869	9.363	78.651	0.177	9.852	78.50
6	0.893	8.993	80.192	0.228	9.584	79.13
7	1.001	8.855	80.641	0.378	9.725	78.94
8	1.440	8.638	81.346	0.832	9.733	78.97
9	2.525	8.522	82.094	2.134	9.715	79.26
10	5.437	8.395	82.835	5.696	9.767	79.73

Table 2. Speed and accuracy of the SE-UTD and Selected STD-UTD predictions for the Handsund profile

Table 2 shows that the SE-UTD has a lower  $E_{rms}$  by about 1 dB and a higher  $THR_m$  by about 1% compared to the extended STD-UTD results. In terms of speed, the SE-UTD performs better than the extended STD-UTD at higher values of  $fnse$ . This may be due to the relative positioning of the selected edges influencing the number of distance and slope distance parameters to be calculated whilst determining the diffraction loss. So the rationale behind the edge selection process described in §2 for the SE-UTD is proven to be effective in terms of accuracy and computation time (albeit at higher values of  $fnse$  for the latter). Fig 3 captures the gist of the results obtained for the Handsund profile and confirms what has been mentioned earlier.

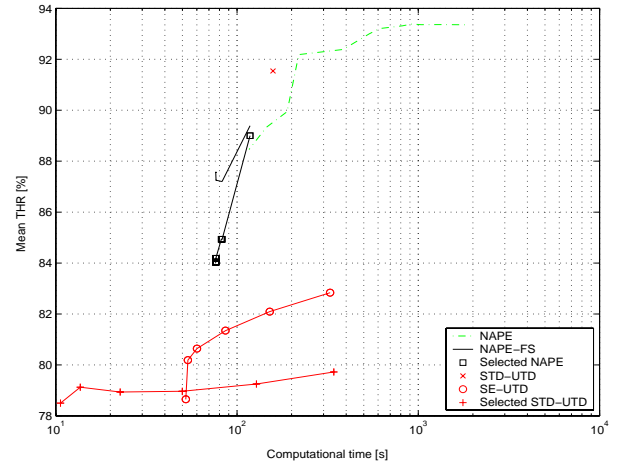


Fig 3. Plot of accuracy against computational time for the models used over the Handsund profile.

**Mjels profile: NAPE-based results.** The optimum  $height\_dom$  determined from the NAPE simulations, is 180m. This is used in the NAPE-FS model and the results are shown in Table 3 below:

$Nse$	Time [min]	NAPE-FS		Selected NAPE	
		$E_{rms}$ [dB]	$THR_m$ [%]	$E_{rms}$ [dB]	$THR_m$ [%]
1	4.05	7.578	91.547	7.929	90.935
2	3.91	7.338	91.667	7.700	90.991
3	3.81	6.877	92.172	7.200	91.586
4	3.64	6.653	92.317	7.021	91.540
5	3.66	6.653	92.317	7.021	91.540

Table 3: Speed and accuracy of the NAPE-FS and NAPE predictions selected at significant regions, in the Mjels profile

The gain in runtime when using the NAPE-FS over the Mjels profile is only about 21% when compared to that of NAPE (with  $height\_dom = 180m$ ). This is because the Mjels profile is quite flat compared to Handsund. Hence most of the terrain occurs within the MFPR; resulting in significant regions with larger widths. Because of the latter effect, it is expected that the NAPE-FS predictions should follow the NAPE predictions quite closely (see Fig 4)

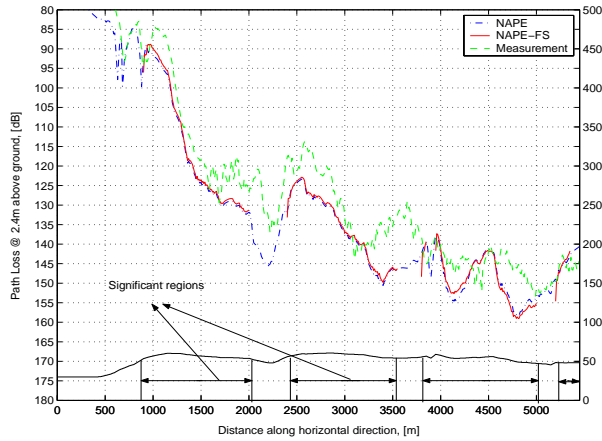


Fig 4: Measurement and predictions from the NAPE and NAPE-FS models for the Mjels profile.

We expect the NAPE-FS model to have a higher absolute value of path loss compared to the NAPE because of the absence of reflections over the free-space zones. However as seen in Fig 4, the NAPE-FS has a slightly lower absolute value of path loss for the first two significant regions and over the segment of 3950m to 5000m. Given that for the Mjels profile, the NAPE predictions overestimate the path loss, the above behaviour of the NAPE-FS predictions causes the NAPE-FS model to have a better performance.

**Mjels profile: SE-UTD-based results.** The SE-UTD model with a value of  $nse = 3$ , has been run over the following segment of the Mjels profile: from 2.0km to 5.45km for a range values of  $fnse$  from 5 to 13 and the results are shown in Table 4.

$fnse$	SE-UTD			Extended STD-UTD		
	Time [min]	$E_{rms}$ [dB]	$THR_m$ [%]	Time [min]	$E_{rms}$ [dB]	$THR_m$ [%]
5	0.51	9.128	78.417	0.10	9.128	78.417
6	0.57	8.358	80.193	0.15	8.358	80.193
7	0.71	7.818	82.008	0.29	7.818	82.008
8	1.07	7.547	82.857	0.67	7.547	82.857
9	2.04	7.375	83.398	1.63	7.375	83.398
10	4.39	7.196	83.900	3.96	7.196	83.900
11	9.94	6.996	84.209	9.57	6.996	84.209
12	24.66	6.791	84.672	24.4	6.791	84.672
13	60.00	6.646	85.097	61.0	6.637	85.097

Table 4. Speed and accuracy of the SE-UTD and Selected STD-UTD predictions for the Mjels profile

The SE-UTD and extended STD-UTD results have the same results for values of  $fnse$  from 5 to 12. This is because the two edge selection approaches have yielded the same set of input edges since the Mjels profile is flat. The usefulness of drawing Fresnel zones across main edges as a means of edge selection, is somewhat mitigated in such circumstances. This can be considered

as a limitation of the edge selection approach used in the SE-UTD model. The SE-UTD model has also been run with a value of  $nse = 5$  but the same results as in Table 4 were obtained. It can be concluded that for a flat profile, an increase in  $nse$  does not result in a greater difference in edge selection between the STD-UTD and SE-UTD.

Although the SE-UTD and extended STD-UTD have the same input edges, the latter has a lower runtime for the small values of  $fnse$ . This is because the pre-processing time corresponding to the edge selection process in the SE-UTD is greater.

## CONCLUSIONS

We have chosen two reference models, the NAPE and the STD-UTD, and applied some modification to the terrain input data to obtain the NAPE-FS and SE-UTD respectively. These have been run on the Aalborg terrain database. A comparison in terms of accuracy and speed has been performed. The NAPE-FS model has brought a gain in runtime with respect to the NAPE model. This gain in runtime is closely related to the shape of the terrain profile. In terms of accuracy, the NAPE-FS has unexpectedly had better performance than the NAPE and the possible reason has been highlighted in this paper. However more simulations have to be run on other databases to monitor the accuracy of the NAPE-FS. The SE-UTD performs better than the extended STD-UTD for profiles with distinctive peaks such as Handsund. However the same improvement is not reproduced for generally flat profiles.

## ACKNOWLEDGEMENTS

We are grateful to Ericsson Ltd. for sponsoring this project and to Aalborg University for the database.

## REFERENCES

1. Levy M F, 1990, Parabolic equation modelling of propagation over irregular terrain, *Elec Lett.*, **26**, 1153-1155.
2. Tzaras C and Saunders S R, 2001, An improved heuristic UTD solution for multiple-edge transition zone diffraction, *IEEE Trans A&P.*, **49**, 1678-1682.
3. Hviid J T et al, 1995, Terrain based propagation model for rural area- An integral equation approach, *IEEE Trans, A&P*, **43**, 41-46.
4. Hristov H D, 2000, Fresnel zones in wireless links, zone plate lenses and antennas, Artech House Publishers, ISBN: 0-89006-849-6.
5. Vogler L E, 1981, The attenuation of electromagnetic waves by multiple knife edge diffraction, NTIA Report 81-86, NTIA Colorado.
6. Owadally A S, Montiel E and Saunders S R, 2001, A comparison of the accuracy of propagation models using hit rate analysis, *IEEE VTC Fall*, **4**, 1979-1983.